PAPER • OPEN ACCESS

Chemical pressure induced substantial negative exchange bias on zero field cooled nanocrystalline $LaFeO_3$

To cite this article: T Lakshmana Rao *et al* 2020 *Mater. Res. Express* **7** 016108

Materials Research Express

OPEN ACCESS

RECEIVED
28 October 2019

REVISED
6 December 2019

ACCEPTED FOR PUBLICATION
27 December 2019

PUBLISHED
13 January 2020

PAPER

Chemical pressure induced substantial negative exchange bias on zero field cooled nanocrystalline $LaFeO_3$

T Lakshmana Rao[1], **M K Pradhan**[1], **Sujay Chakravarty**[2] and **S Dash**[1]

[1] Dept. of Physics and Astronomy, National Institute of Technology Rourkela, Rourkela, Odisha 769008, India
[2] UGC-DAE Consortium for Scientific Research, Kalpakkam Node, Kokilamedu 603104, India

E-mail: dsuryanarayan@gmail.com

Keywords: lanthanum ferrite, exchange bias, chemical pressure, nanocrystal

Supplementary material for this article is available online

Abstract

We report a distinctly different zero feld cooled negative exchange bias(EB) effect in Ni doped $LaFeO_3$ nanoparticle where the EB field is both temperature and concentration dependent. Nanoparticles of Ni substituted $LaFeO_3$ is prepared by a sol-gel process. The broadening of diffraction peaks with Ni is due to the combined effect of octahedral distortion and reduction in particle size while rulling out any structural phase change. A substantial EB is acquired below spin reorientation transitions which further reduces with higher chemical pressure of Ni. EB field is found to be ~5.71 kOe at 5 K, revealing a large value compared to similar zero field cooled EB systems. A simple model is proposed based on tunable shell-core magnetic phases to explain these unique EB effects. Present study also aimed to explore the spin and oxidation state of Fe vis a vis magnetic ordering in $LaFeO_3$ together with consequence of Ni doping.

1. Introduction

Exchange bias (EB) can be usually identified by shifting of the hysteris loop along the magnetic field(H) axis. As a nonequilibrium phenomena, it depicts an interface couling among different magnetic orderings, such as ferromagnetic (FM)-antiferromagnetic (AFM) [1], FM-spin glass (SG) [2], AFM-ferrimagnetic (FEM) [3] and FM-FEM [4] after cooling the system in a static magnetic field through the Néel temperature (T_N) of the AFM or spin glass temperature (T_{SG}) [5]. Such an effect is applied in designing ultrahigh-density magnetic recording and spin valve devices [6, 7]. The underlying physics of the EB is the exchange interaction between different magnetic orders. In an usual AFM-FM interface, the orientation of the AFM spin is weakly influenced by H, while in a soft FM, which is strongly exchange-coupled to the AFM will have its interfacial spins pinned. The energy associated with the process of reversal of the FM's moment results a Néel domain wall within the AFM. This extra energy term implies a shift in the switching field of the FM [1]. A representative system of EB system is Co–CoO [1], where the EB occurs at the interface of Co(FM) and CoO(AFM) with a maximum EB field is 9.5 kOe. Recently, the EB effect was studied in two different systems, Pr doped $LaCrO_3$ and Sr_2YbRuO_6, in which the cooling field and temperature dependent positive and negative EB effects is observed [8, 9]. In these cases, the EB effect is completely different from what appears in bilayer and other interface structures. The coupling between the Pr^{3+} and Cr^{3+} at different atomic sites determines the EB effect in $La_{1-x}Pr_xCrO_3$ where as in Sr_2YbRuO_6, the EB effect originates from the Dzyaloshinsky–Moria interaction induced FM and AFM coupling between Yb^{3+} and Ru^{3+}, which are in the same atomic site in the ABO_3 structure [8, 9]. In a similar context, tuning of exchange bias is also observed in a core–shell nanoparticles of FeO/Fe_3O_4, where the dimensions of core–shell determines not only the corercivity and exchange bias but also act as a dominant reversal mechanism of the FEM Fe_3O_4 [10]. Therefore, it is likely that the EB effect may be observed in some other similar systems irrespective of the subtle origins.

To explore new materials with EB based on this idea, we have chosen to study nanoparticles of Ni doped in $LaFeO_3$, considering that the Ni^{3+} spins enter into FM/weak FM(WFM) ordering, while Fe^{3+} is in the AFM state

at low-T. Normally with homovalent Ni doping in similar oxides, the parent transition metal is shown to improve its valence state, resulting in a mixed valence states in the system [11, 12]. In a system like $PrFe_{1-x}Ni_xO_3$, an evidence of a transition of the Fe^{3+} from high spin to low spin configuration with Ni content is also present [13]. In these systems, the electrical conduction is primarily due to hoping of the electrical carriers between their localized states and mostly are magnetically ordered insulators inclusive of $LaFeO_3$ [14]. $LaFeO_3$ exhibits AFM ground state with a high neel temperature around $T_N \sim 740$ K [15, 16], however, with substitutions and/or size reduction to nano meter, the magnetic ordering changes to weak FM. Our results show that both a positive and a large negative EB (~5.71 kOe at 5 K) effect is observed at different temperatures well below T_N but especially cooling in zero field. This zero field cooled exchange bias (ZEB) effect is distinctly different from the conventional field cooling EB where external magnetic field is essential in creating the unidirectional anisotropy during the cooling process. This ZEB effect can be further tuned by varing Ni concentration in $LaFeO_3$. A simple model is proposed to explain this ZEB effects. The present study also aimed to explore the spin and oxidation state of Fe and its magnetic ordering in $LaFeO_3$ together with the consequence of Ni doping.

2. Experimental procedure

A series of Ni doped $LaFeO_3$ nanoparticle were prepared by sol-gel technique. High purity raw materials of $La(NO_3)_3{\cdot}6H_2O$, $Fe(NO_3)_3{\cdot}9H_2O$, $Ni(NO_3)_3{\cdot}6H_2O$, citric acid ($C_6H_8O_7$) and ethylene glycol ($C_2H_6O_2$) from Sigma Aldrich, were taken as precursor materials. Stoichiometric amounts of individual metal nitrates were dissolved in Millipore water and added through continuous stirring. The solution was heated to a mild temperature to ensure evaporation of nitrate fumes followed by addition of citric acid in a (metal ion: citric acid) 1:1 molar ratio with continuous stirring. The pH of the citrate solutions was than maintained at 7 by adding ammonia solution. The solution was heated for several hours until it becomes a viscous mass. Ethylene glycol was than added in the ratio of (metal:ethylene glycol) 1:1.2 into the viscous mass and was heated in a temperature range of 60 to 200 °C for gelation. Auto combustion of gel leaving behind organic based, black fluffy precursor powder. The resulting powder was calcined at 400 °C for 3 h. The calcined powders were reground and then pressed into pellets, subjected to sintering at 700 °C for 3 h to obtain a final samples for characterizations. Synchrotron-based powder x-ray diffraction measurements were carried out on well-ground powder samples at Extreme Conditions Angle Dispersive/Energy dispersive x-ray diffraction (EC-AD/ED-XRD) beamline (BL-11) at Indus-2 synchrotron source, Raja Ramanna Centre for Advanced Technology (RRCAT), Indore, India. The details of the experiment can be found elsewhere [16]. Microstructures and morphology have been investigated using field emission scanning electron microscopy (FESEEM). The temperature dependent magnetization measurements (M-T) and first harmonic ac-susceptibiity at 3 Oe are measured using SQUID-VSM(M/s. QD, USA). Mossbauer measurement has been carried out using transmission ^{57}Fe Mossbauer spectrometer at room temperature and fitted with MossWinn program. From here onwards the terminology used for the samples $LaFeO_3$ as LFN0, $LaFe_{0.9}Ni_{0.1}O_3$ as LFN1, $LaFe_{0.7}Ni_{0.3}O_3$ as LFN3 and $LaFe_{0.5}Ni_{0.5}O_3$ as LFN5, will be followed, unless it is stated differently.

3. Results and discussions

3.1. Structural and morphological analysis

For the basic characterizations of materials, we have performed synchortron XRD and FESEM. For strutural information, synchrotron radiation based XRD is taken to detect undesired phase if any in the samples with experimental acuuracy. The Rietveld refinement of the room temperature XRD patterns are shown in figures 1(a)–(d). Quantitative phase analysis revealed the distorted orthorohmbic structure of the samples with ***Pbnm*** space group without any detectable impurity. With Ni concentration, the peaks gets broadened, may be a combined effect of octahedral distortion and reduction in particle size. A schematic of the unit cell of a representative sample LFN3 is depicted in the figure 1(e). Here, Fe^{3+}/Ni^{3+} ions occupy the 4b site which are surrounded by six neighbouring O^{2-} ions forming FeO_6 octahedra. These corner sharing FeO_6 octahedrons remain tilted a few degee about the direction of the *c*-axis. Furthermore, As shown in figure 1(f), the most intense peaks shifts towards higher diffraction angles. The shifting and decrease in cell volume with the increase in Ni concertation is a consequence of smaller Ni^{3+} (0.56 Å) ion replacing exactly the larger Fe^{3+} (0.645 Å) in the unit cell. There is no evidence of any structural phase change caused due to chemical pressure exerted by Ni^{3+} in the $LaFeO_3$ host thereby ruling out the the possible compositional phase change in the range $0 \leqslant x \leqslant 0.5$. The shrinkage of unit cell volume may reduce the Fe–O bonds in the FeO_6 octahedra and results in rise in their distortions, as shown in table S1 (see supplementary material is available online at stacks.iop.org/MRX/7/016108/mmedia).

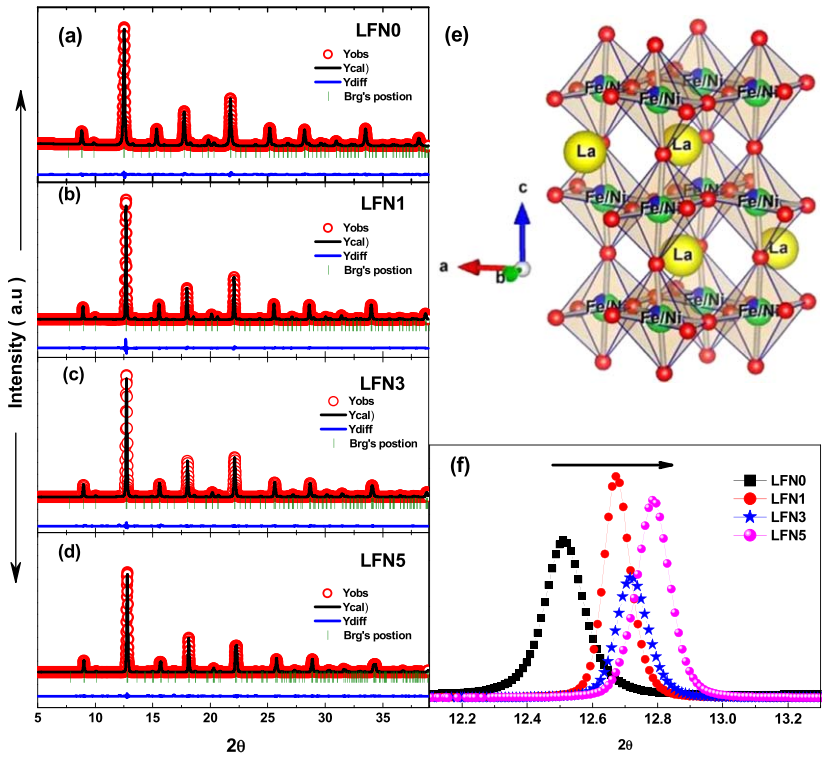

Figure 1. (a)–(d) Synchrotron energy dispersive x-ray diffraction and Rietveld refinements of the Ni doped $LaFeO_3$, (e) Distorted orthorhombic perovskite unit cell of LFN3, (f) compositional variation of main peak.

To explore the surface morphology which is expected to be an integral part of the substitution induced change in properties of $LaFeO_3$, FESEM was used. Figures 2(a)–(d) shows FESEM micrographs of the samples. As shown in figure 2(a), for LFN0, mostly the particles are agglomerated, with a mean particle size of 52 nm. However, nickel-doped nanoparticles connect with each other to form a large network system of irregular size and shapes with an average particle size of around the 35–23 nm (see table S1: supplementary material) in an aspherical morphology as depicted in figures 2(b)–(d). It may be due to a large number of escaping gases from the rapid decomposition of organic compounds and strong redox reaction during sol-gel auto combustion method. The particle size is found to decrease with increase in Ni concentration. In order to shed light more on the issue of morphology, individual elemental maping is carriedout in FESEM (see supplementary material). The EDX spectrum additionally confirms that there exist nearly stoichiometric amount of O, Fe, Ni and La elements inside the selected area and with no detectable impurity (see figure S1, supplementary material).

3.2. Magnetic studies

To know the effect of chemical pressure vis-à-vis particle size on the magnetic state, temperature(T)-dependent magnetization(M) data were acquired under zero-field-cooled (ZFC) and field-cooled (FC) conditions. As shown in figure 3, initially, each sample was cooled under a nominal zero field to 5 K. Then, a field of 500 Oe field was applied. The magnetization data (ZFC) were collected as the sample was warmed to 300 K, and the FC data were collected as the sample was cooled to 5 K (at 500 Oe). As shown in figure 3(a), the nature of ZFC and FC curve of LFN0 are similar but FC posseses a higher magnetization which is already documented in our earlier literatures [15–17]. However, the ZFC and FC for LFN1 and LFN3 show an irreversible magnetic behavior at irreversibility (T_{irr}) temperature but below room T. Nonethless, this is mostly defined as the T at which the ZFC and FC split and corresponds to the blocking temperature of the largest nanoparticles in the superparamagnetic systems. Here one notice, even ZFC and FC is not merge at 300 K for LFN1, as exected since the neel temperature(T_N) is much above 300 K for the parent sample. In LFN3, as the temperature increases in ZFC measurement, firstly, the M_{ZFC} increases and then achieves a maximum value at T_B. Above T_B, in the unblocked region, the M_{ZFC} monotonically decreases with increasing T. This is the characteristic behavior of superparamagnetic materials. Further higher Ni doping (50%), drastically alters the magnetic behavior of $LaFeO_3$. It shows a normal paramagnetic behavior with a nominal changes in the values of ZFC and FC, due to field history of the sample except a peak around 10 K in ZFC path(inset of figure 3(d)). It may be due to blocking of spin while lowering temperature. However the same is diminished in FC path, may due to effect of cooling field. The detail of such transition around 10 K in ZFC will be discussed in the later part of the section.

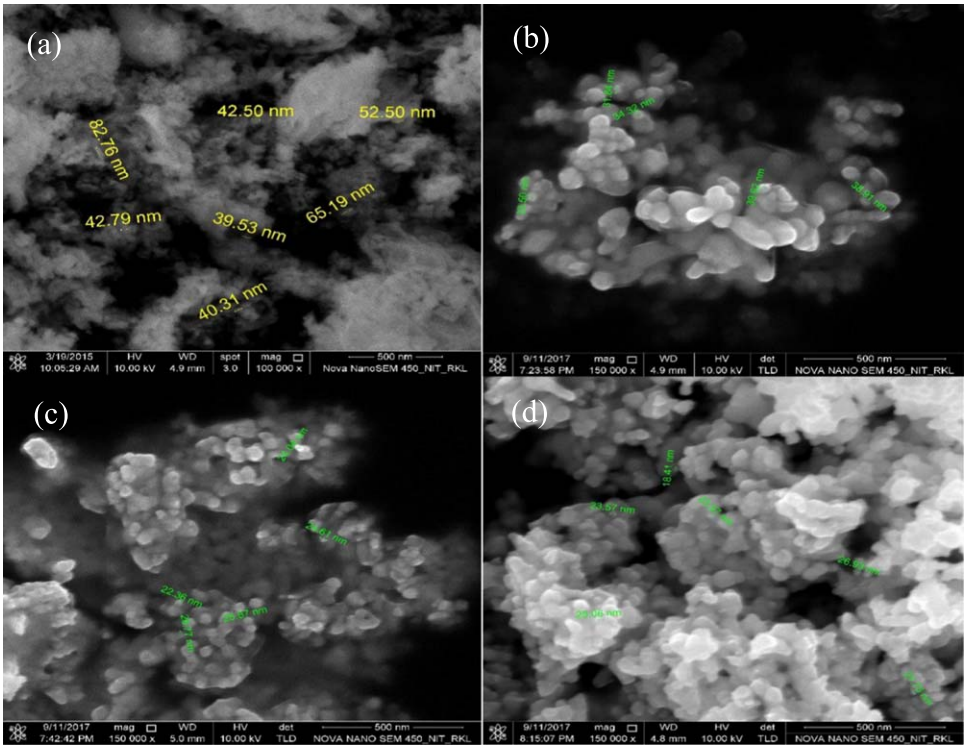

Figure 2. FESEM micrographs of (a) LFN0, (b) LFN1, (c) LFN3 and (d) LFN5 respectively.

To know the exact field dependent magnetic behavior of all samples, isothermal magnetization is measured at 300 K and 5 K. The thermo magnetic hysteresis loops are measured in the protocols: 0 $\rightarrow$ 70 kOe $\rightarrow$ -70 kOe $\rightarrow$ 70 kOe at 300 K and 5 K. From the figure 3(e), at 300 K, the magnetization value achieved at 70 kOe starts increasing upto 30% Ni and than falls. This falls may be due to disorder arises from the competing interactions between Ni and Fe spins as each of having equal spin levels. However, these samples shows an intriguing effects once we magnified the hysteresis data around zero field. The enlarge view of the displaced M–H loops are shown in figure 4(a). The hysteresis loops are found to be highly asymmetric at 300 K, suggesting the exchange bias effects. Usually, the exchange bias field H_{EB} is defined as $H_{EB} = |H_1 + H_2|/2$ and coercive (H_C) is defined as $H_C = |H_1 - H_2|/2$, where H_1 and H_2 are the left and right coercive fields, which is rather the intercepts of M on the –ve and +ve side of the H-axis. Correspondingly, the vertical magnetization shift (M_{Shift}) is defined as $M_{Shift} = |M_1 + M_2|/2$, where M_1 and M_2 are the upper and lower remanent magnetizations.

For 300 K. the H_{EB} is highest for LFN3 where as H_C is highest for LFN1. However, this effect drastically changes at 5 K. As shown in figure 4(b), The hysteresis loops are obtained after zero field cooled process suggesting zero field cooled exchange bias(ZEB). The assymetric hysteresis loops are completely shifted towords negative field axis which is very rare. The $H_{ZEB} = 5.71$ kOe in LFN3 is considered to be a very high ZEB [18–20]. The $H_{ZEB} = 1.143$ kOe is considered to be a medium range in EB [18–20]. The variations of exchange bias parameters as a function of doping concentrations is shown in figures 4(c) and (d) at two different temperatures.

Such a high value has many application prospects in designing ultrahigh-density magnetic recording, giant magnetoresistance, and spin valve devices [6]. From figure 4(d), at 5 K the H_{EB} and H_C is found to be the highest for LFN3 among all the samples signifies the better applicability around this doping level.

The increase of H_{EB} and Hc at Ni 30 suggests a strong exchange coupling between Fe and Ni resulting a weak FM state. After that, this values decreases. The possible reason may be stated in this way. The non-zero value of the EB is attributed to the presence of exchange coupling between the WFM-like shell and AFM-like core of the nanoparticles [21, 22]. For nanosized particles, mostly the surface spin act as a WFM on AFM core. So due to the coupling between surface WFM and AFM at the core, the WFM spins will try to drag AFM spins to the external fields and produce additional exchange bias fields besides that in the core, which results in a larger H_{EB} [21, 22]. Here the H_C and H_{EB} for doping system are much larger than $LaFeO_3$ except for LFN5. As Ni doping increases, the decreasing particle size increases the FM phase fractions leading to the rise of total anisotropy energy which may causes the enhancement of coercivity [22]. The WFM and AFM phase coexistence in a single nanoparticles leads to the usual FM/AFM interfaces (as in other similar systems), when the sample is cooled from 300 K down to 5 K. With lowering of temperature, the exchange bias effect significantly increases. This enhancement of this EB can be ascribed to the increase of the interfacial WFM–AFM interaction.

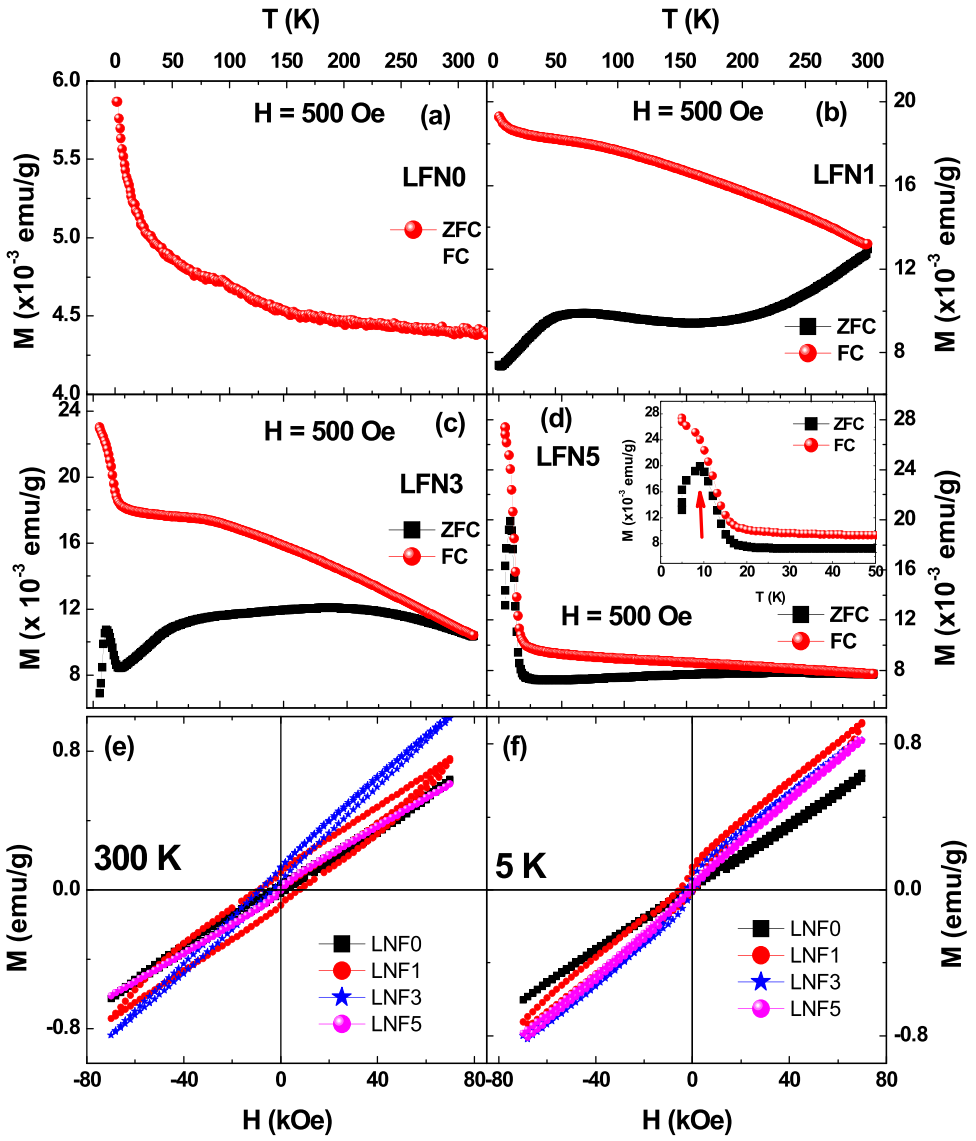

Figure 3. M versus T at fixed field of for (a) LFN0, (b) LFN1, (c) LFN3, (d) LFN5. Isothermal magnetization at (e) 300 K and (f) 5 K for all samples.

With higher Ni substitutions, the relative phase component of WFM enhances at the cost of AFM phase (Note: the parent system $LaFeO_3$ shows AFM ground state). Due to this, the ferromagnetic anisotropy increases and the relative phase component of WFM and AFM in these systems play a vital role in determining the magnitude of EB and coercive fields. To know the low temperature magnetic state of LFN5 in detail, AC-susceptibility measurement is carriedout. As shown in figure 5, the frequency dependent real and imaginary part of susceptibility is measured at very low field of 3 Oe. As in figures 5(a), (b) the peaks shift to lower temperature with decreasing frequencies. Also for intensities, the real and imaginary (may not be trivial due to small values) components, the peaks decreases with decreasing frequencies. This behaviour of χ' and χ'' is typical of a spin glass state [23].

3.3. Mossbauer studies

The above description of relative phase fractions of magnetic orders to EB in these systems can be firmly established by using Mossbauer spectra. Figure 6(a) depicts the ^{57}Fe Mossbauer spectra of LFN0. The spectrum consists of the intrinsic six lines of the orthoferrites. The Mossbauer spectra of LFN1 and LFN3 are well fitted by single sextets where as LFN5 by a sextet and a singlet as shown in the figures 6(b)–(d).

The Mossbauer spectra shows sagging as the nickel doping concentration percentage increase in the samples. The calculated parameters of the spectra from the curve fitting using MOSSWIN software are tabulated in the table 1. The isomer shift (IS) values are observed to decrease consistently with the increase in Ni content which are influenced by the shielding effect in the nano crystalline samples. The isomer shift is influenced by the S

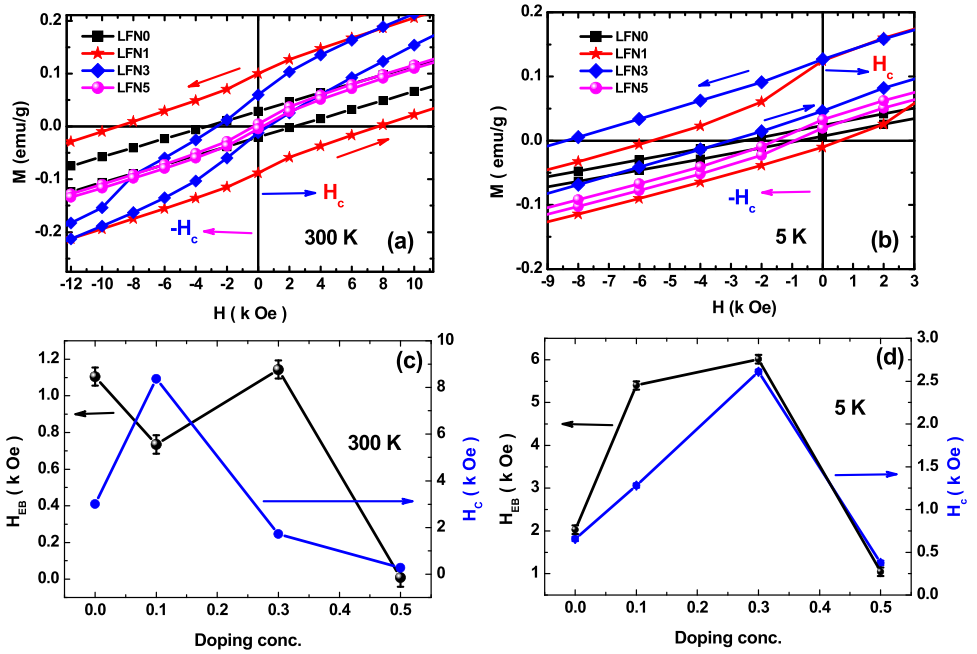

Figure 4. M versus H at (a) 300 K and (b) 5 K showing exchange bias effect. The respective exchange bias field and coercive field w.r.t doping concentrations at (c) 300 K and (d) 5 K.

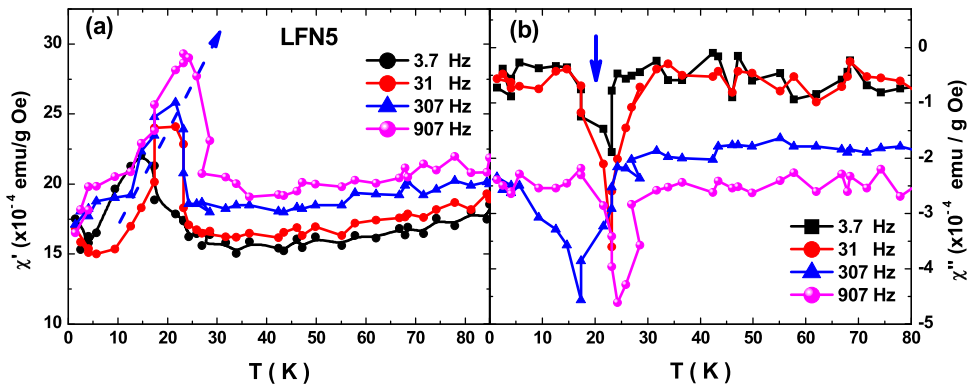

Figure 5. Frequency dependent first order real(a) and imaginary(b) part of χ versus T for LFN5

electron density at a nucleus. The marginal reduce in 'IS' specifies that there may be a reduce in the unit cell volume with Ni on the Fe site, which is consistent with our XRD analysis [24].

The observed value of the hyperfine field (B_{hf}) ~ 52 T, isomer shift (IS) ~0.4 mm s^{-1} and quadrupole splitting (QS) ~ 0.042 mm s^{-1} of the LFN0 are consistent with the literature [25]. The QS is an extremely sensitive and prone to local site symmetry and the observed small QS in the LFN0 ascertain the octahedral environment of Fe without any significant distortion. As the Ni doped at Fe sites, the QS is marginally increased. This may be caused due to the change in O environment upon Ni doing at Fe octahedral sites, which assure that the iron ions are subjected to a non-cubic electric filed gradient [26].

One may notice that the volume shrinkage may affect the Fe–O distance is evidenceing from the isomer shift [27]. This lead to the distortion of the FeO_6 octahedra ratio in a magnetically ordered state. The FeO_6 octahedra is progressively distorted due to chemical pressure as the Ni concentration increases, there is formation of bonds Fe–O–Fe, Fe–O–Ni and the introduction of new bond lengths of Fe–O and Ni–O, due to which the crystal field splitting energy (CFS) may gradually increased. The isomer shift value for all sextets in samples LFN0, LFN1 and LFN3 are typical for high spin Fe^{3+} in octahedral coordination. This establishes that Fe cations exists in the 3 + oxidation state in the LFN0, LFN1 and LFN3 samples. Note that, the oxidation state of La, Fe and Ni are obtained as 3+, 3+ and 3+ respectively by using x-ray photoelectron spectroscopy (see figure 2 and discussions in supplementary material), For the LFN5 sample the Mossbauer spectrum shows a singlet and a small area sextet (see table 1). One may infer that LFN5 conatins a major fraction of disordered magnetic phase that may be

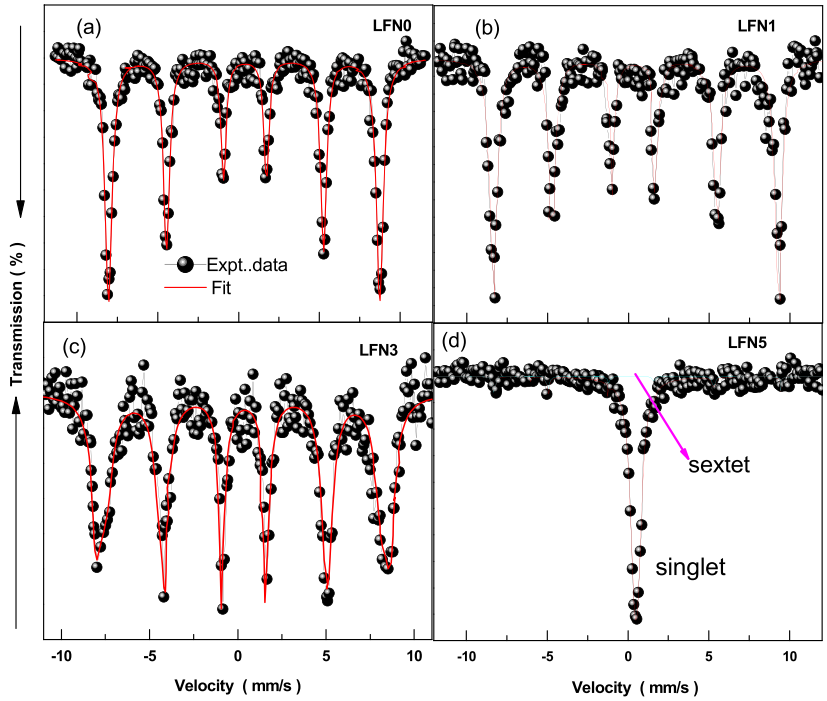

Figure 6. Room temperature Mossbauer spectra of LFN0, LFN1, LFN3 and LFN5 nanomaterials.

Table 1. Mossbauer spectra with fitted parameters of the Ni doped nano particles.

Splitting	B_{hf} (Tesla)	Width (mm s^{-1})	Area (%)	Isomer shift (mm s^{-1})	Qua (mm s^{-1})
LFN0					
1st Sixlet	51.98 ± .015	0.412 ± .022	100	0.392 ± .0027	0.042 ± .0079
LNF1					
1st sextet	50.57 ± .0492	0.51 ± .02	100	0.37 ± .0067	0.0829 ± .013
LNF3					
1st Sextet	48.50 ± .23	0.62 ± .11	100	0.35 ± .044	0.282 ± .0812
LNF5					
1st Sextet	34.50 ± .23	0.21 ± .10	7.28%	0.34 ± .041	0.296 ± .0723
Singlet		0.60 ± .015	92.72%	0.49 ± .0085	0.257 ± .0213

a spin glass or simply paramagnetic phase which will be clarified from the isothermal magnetic measurements. The LFN0 is anti-ferro magnetically ordered below ~740 K. The iron ions are arranged as two sub lattices are slightly canted with respect to the antiferromagnetic axis, resulting in a small net magnetic moment. The increase in Ni doping concentration affects aniferromagntic interaction, which is attributed to reduce in internal magntic filed experienced as a result of fall in number of ions. The internal magntic filed is very less in the case of the LFN5 sample as compared to other samples [25].

4. Conclusions

To sum up, a large but zero feld cooled negative exchange bias (ZEB) effect is observed in Ni doped $LaFeO_3$ nanoparticle, which exhibits a similar relationship of the H_{EB} and H_C at low temperature, while different at higher temperature. For 30% Ni, this exhibits the highest vales. In these nanoparticles, this phenomenon can be ascribed to the interfacial exchange coupling between WFM regions and AFM boundaries created by antisite disorders in a core–shell like structure with AFM core and WFM shell. The magnetization of $LaFeO_3$ is considerably enhanced due to substitution of Ni. The EB effect, exchange anisotropy is very prominent in the 30% Ni doped sample. Considerably high value of EB effect (~5.71 kOe) in the 30% Ni in a multiferroic $LaFeO_3$ would be quite interesting in different switching as well as in other recording devices. as the EB effect is used to pin the state of the readback heads at exactly their point of maximum sensitivity. Such study will certainly help in searching new materials for practical applications related to similar EB effect.

Acknowledgments

We would like to acknowledge Dr V R Reddy of UGC-DAE CSR, Indore for Mossbauer measurement. Dr V Srihari of RRCAT, Indore is acknowledged for synchrotron XRD measurement. One of the authors M K Pradhan acknowledges UGC-DAE CSR Mumbai for Fellowship under the project grant of CRS/M/226.

ORCID iDs

T Lakshmana Rao https://orcid.org/0000-0003-1831-1934
S Dash https://orcid.org/0000-0002-6278-2277

References

[1] Meiklejohn W H and Bean C P 1956 New magnetic anisotropy *Phys. Rev.* **102** 1413–4
[2] Mannan Ali P, Adie C H, Marrows D, Greig B J, Hickey and Stamps R L 2007 Exchange bias using a spin glass *Nat. Mater.* **6** 70–5
[3] Salazar-Alvarez G, Sort J, Surin˜ach S, Baro M D and Nogué J 2007 Synthesis and size-dependent exchange bias in inverted core–shell MnO|Mn_3O_4 nanoparticles *J. Am. Chem. Soc.* **129** 9102–8
[4] Cain W C and Kryder M H 1990 Investigation of the exchange mechanism in NiFe-TbCo bilayers *J. Appl. Phys.* **67** 5722–4
[5] Nogués J and Schuller I K 1999 Exchange bias *J. Magn. Magn. Mater.* **19** 2203–232.
[6] Wang B M, Liu Y, Ren P, Xia B, Ruan K B, Yi J B, Ding J, Li X G and Wang L 2011 Large exchange bias after zero-field cooling from an unmagnetized state *Phys. Rev. Lett.* **106** 077203–4
[7] Noguésa J, Sort J, Langlais V, Skumryev V, Suriñach S, Muñoz J S and Baró M D 2005 Exchange bias in nanostructures *Phys. Rep.* **422** 65–117
[8] Yoshii K 2011 Positive exchange bias from magnetization reversal in $La_{1-x}Pr_xCrO_3$ ($x \sim 0.7$–0.85) *Appl. Phys. Lett.* **99** 142501–3
[9] Singh R P, Tomy C V and Grover A K 2010 Observation of tunable exchange bias in Sr_2YbRuO_6 *Appl. Phys. Lett.* **97** 182505
[10] Xiaolian S, Huls N F and Shouheng S A S 2012 Tuning exchange bias in core/shell FeO/Fe_3O_4 nanoparticles *Nano Lett.* **12** 246–51
[11] Sánchez M C, García J, Blasco J, Subías G and Perez-Cacho J 2002 Local electronic and geometrical structure of $LaNi_{1-x}Mn_xO_{3+\delta}$ perovskites determined by x-ray-absorption spectroscopy *Phys. Rev.* B **65** 144409–144409
[12] Gutierrez D, Pena O, Dura P and Mourea C 2002 Crystal structure, electrical conductivity and seebeck coefficient of Y (Mn, Ni) O_3 solid solution *J. Eur. Ceram. Soc.* **22** 567–72
[13] Makhdoomi A B, Ikram M and Kumar R 2010 Mossbauer studies and magnetic studies of Ni doped orthoferrites $PrFe_{1-x}Ni_xO_3$ ($x \leqslant 0.3$) *J. Magn. Magn. Mater.* **322** 2581–4
[14] Rao C N R, Parkash O and Ganguly P 1975 Electronic and magnetic properties of $LaNi_{1-x}Co_xO_3$, $LaCo_{1-x}Fe_xO_3$ and $LaNi_{1-x}Fe_xO_3$ *J. Solid State Chem.* **15** 186–92
[15] Lakshmana Rao T, Pradhan M K, Goutam U K, Siruguri V, Reddy V R and Dash S 2019 Substitution induced magnetic phase transitions and related electrical conduction mechanisms in $LaFeO_3$ nanoparticle *J. Appl. Phys.* **126** 064104–12
[16] Lakshmana Rao T, Pradhan M K, Siruguri V and Dash S 2019 Doping-induced modifications in the magnetoelectronic properties in $LaFeO_3$ nanoparticles *J. Super. Nov. Magn.* (https://doi.org/10.1007/s10948-019-5138-9)
[17] Lakshmana Rao T, Pradhan M K, Chandrasekhar M, Ramakrishna P V and Dash S 2019 Structural, magnetic, grain and grain boundary mediated conduction features of low dimensional $LaFeO_3$ nanoparticles *J. Phys.: Condens. Matter* **313** 45803–11
[18] Krishna Murthy J and Venimadhav A 2013 Giant zero field cooled spontaneous exchange bias effect in phase separated $La_{1.5}Sr_{0.5}CoMnO_6$ *Appl. Phys. Lett.* **103** 252410–5
[19] Han Z D, Qian B, Wang D H, Zhang P, Jiang X F, Zhang C L and Du Y W 2013 Magnetic phase separation and exchange bias in off-stoichiometric Ni-Mn-Ga alloys *Appl. Phys. Lett.* **103** 172403–5
[20] Maity T, Goswami S, Bhattacharya D and Roy S 2013 Superspin glass mediated giant spontaneous exchange bias in a nanocomposite of $BiFeO_3$-$Bi_2Fe_4O_9$ *Phys. Rev. Lett.* **110** 107201–5
[21] Keller J, Miltenyi P, Beschoten B, Güntherodt G, Nowak U and Usadel K D 2002 Domain state model for exchange bias. II. experiments *Phys. Rev.* B **66** 014431
[22] Mukhopadhyay K, Mahapatra A S and Chakrabarti P K 2013 Multiferroic behavior, enhanced magnetization and exchange bias effect of Zn substituted nanocrystalline $LaFeO_3$ ($La_{(1-x)}Zn_xFeO_3$, $x = 0.10$ and 0.30) *J. Magn. Magn. Mater.* **329** 133–41
[23] Mydosh J A 1993 *Spin Glasses: An Experimental Introduction* (London: Taylor & Francis)
[24] Makhdoomi A B, Ikram M and Kumar R 2010 Mossbauer studies and magnetic studies of Ni doped orthoferrites $PrFe_{1-x}Ni_xO_3$ ($x \leqslant 0.3$) *J. Magn. Magn. Mater.* **322** 2581–4
[25] Eibschutz M, Shtrikman S and Treves D 1967 Mossbauer studies of Fe^{57} in orthoferrites *Phys. Rev.* **156** 562–77
[26] Tiwari Ashutosh 1998 Local environment of Fe in $NdFe_{1-x}Ni_xO_{3-\delta}$ perovskite oxides *J. Alloys Compd.* **274** 42–6
[27] Hearne G R, Pasternak M P, Taylor R D and Lacorre P 1995 Electronic structure and magnetic properties of $LaFeO_3$ at high pressure *Phys. Rev.* B **51** 11495–500